Computer Modeling of Transverse Residual Stresses in Repair Welds

Transverse stress distributions are found to display almost yield magnitude at the repair surface, but decrease to zero with depth

BY R. H. LEGGATT

ABSTRACT. A theoretical investigation of the effects of structural restraint, repair depth and wall thickness on the distribution of transverse residual stresses at repair welds in heavy-section plates and cylindrical structures has been conducted using a computer program. The applicability of the program was demonstrated by comparison with experimental measurements at a 28-mm-deep repair weld in a 75-mm-thick carbon-manganese steel test panel. The computed stresses were in good agreement with the experimental results, and the analysis showed why the net membrane stress in the panel at the repair weld was compressive.

The program was then used to investigate the effects on the residual stress distribution of the different levels of restraint present at repairs of various lengths in flat plates, and at full length axial repairs, full circumferential repairs and part-circumferential repairs in cylinders. It was also used to investigate the effects of repair depth and wall thickness. In nearly all cases, the stresses were computed to be of yield magnitude in tension at the repaired surface and to decrease with depth from the surface.

Introduction

Knowledge of the residual stress distribution in repair welds is necessary in order to make an accurate determination of the tolerable size of any remaining defects, and to assess the risk of crack growth in service. Defects in the repair weld or its heat-affected zone, or unrepaired defects in the original weld, are most commonly oriented parallel to the welding direction. Hence, residual stresses transverse to the repair weld are of particular interest. This paper describes the results of a parametric study of the effects on the distribution of transverse residual stresses in repair welds of restraint, repair length and depth, plate thickness and vessel curvature. The study was carried out using The Welding Institute computer program TRAN1, which models the development of transverse stresses during the deposition of successive weld passes. Program TRAN1 provides a simplified one-dimensional model of the complex thermomechanical elastic-plastic processes occurring during welding. It requires experimental validation under conditions relevant to the materials, geometry and welding conditions being investigated. In the present project, this validation was provided by modeling the deposition of an experimental repair weld in which the residual stress distribution had previously been measured (Ref. 1).

Computer Program TRAN1

TRAN1 is an in-house The Welding Institute computer program that models the development of transverse stress and strain during the deposition of a restrained multipass butt joint weld. The weld is represented in the model by a one-dimensional array of bar elements each of which transmits a uniform transverse stress across the joint. This simplification of the actual three-dimensional stress state is necessary in order to reach a solution for a series of time steps during each pass of a multipass welding procedure within a reasonable computing time. All those factors that were believed by the author to have a significant effect in controlling the transverse stresses were allowed for in the model, including the heat flow due to the weld; the mechanical response of the heated metal under conditions of changing strain, temperature and loading direction; external restraint due to the configuration of the structure being welded; internal restraint due to differential distortions between sections ahead of and behind the weld pool; and yield interaction between longitudinal and transverse stress. The program was originally written to calculate stresses at long welds in flat plates subject to uniform restraint, but can be used to model other welding configurations, such as repair welds or welds in cylinders by applying an appropriate level of restraint.

TRAN1 has previously been validated by comparison with experimental measurements of residual stresses and distortions at welded butt joints in 50-mm (2-in.) thick austenitic stainless steel plate (Ref. 2). The program was found to give good agreement with experimental results for a wide range of heat inputs, numbers of passes, degrees of restraint, and edge preparations for both submerged arc and shielded metal arc multipass groove welds. Where differences between computed and measured stresses occurred, the program generally gave conservative estimates of the distortions or stresses.

In the present project, TRAN1 has been used to calculate residual stresses at repair welds in carbon-manganese and low-alloy steels. As these conditions were significantly different from the original validation data, it was necessary to provide additional validation for the program with respect to internal residual stresses measured in a repair weld in C-Mn steel.

KEY WORDS

Computer Modeling
Structural Restraint
Repair Welds
Transverse Residual Stress
Repair Depth
Wall Thickness
Heavy Section Plates
Cylindrical Structure
Computed Stresses
Residual Stress Distribution

R. H. LEGGATT is with The Welding Institute, Abington Hall, Abington, Cambridge, U.K.

Paper presented at a seminar of IIW Commission X, during July 1988.

Experimental Validation of TRAN1 by Comparison with Data from Panel W20

Repair-Welded Panel W20

The distribution of residual stresses in a repair weld in a panel designated W20 was used to demonstrate the applicability of program TRAN1 with respect to repair welds in C-Mn steels. The base plate for W20 was 75-mm (3-in.) BS 1501:224 Grade 430 LT50 aluminum-treated carbon-manganese steel. The panel geometry is shown in Fig.1 and a cross-section of the original weld and repair weld is shown in Fig. 2. The original weld was a full length double V-groove submerged arc weld made using Oerlikon SD3 wire and OP41TT flux. After welding, the panel was fitted with three strongbacks and heat treated at 600°C (1112°F) for six hours. The repair cavity was then excavated by air carbon arc gouging followed by hand grinding to a maximum depth of 27 mm (1.06 in.). The cavity was filled in the overhead position using the "two-layer" (Refs. 3–5) technique to refine the HAZ microstructure. Carbon-manganese Tenacito R electrodes (E7018 type) of 3.2- and 4-mm (⅛- and 5/32-in.) diameters were used. A total of 84 weld passes was required to fill the cavity and deposit a layer of temper beads at the surface. The temper beads, whose purpose was to reheat the underlying passes, were subsequently ground off to leave a flat surface. The material compositions, mechanical properties and welding conditions are summarized in Tables 1 to 3.

The through-thickness distributions of internal residual stresses in Panel W20 were measured at 13 different locations at various positions along the length and across the width of the repair weld. The residual stresses were measured by a sectioning method, based on a procedure described by Rosenthal and Norton (Ref. 6), which involves the splitting and layering of strain gauged blocks removed from the specimen. It is difficult to obtain a rigorous estimate of the accuracy of this procedure. In the author's experience, internal residual stress measurements usually contain scatter or apparent inconsistencies of up to 15% of the peak measured stress. The majority of this is thought to be due to inherent variability of the stress rather than experimental error.

The transverse residual stresses were found to vary only slightly across the width of the repair weld, with the highest values on the weld centerline. The internal stress distributions were found to be fairly constant along the length of the weld, except near the ends where the depth of the cavity and of the tensile stress zone both decreased. The measured distributions of internal transverse stresses in the central portion of the weld length (at 80 and 240 mm — 3.1 and 9.5 in.— from the middle of the panel) were used as a basis for assessing the validity of the theoretical transverse stress distribution calculated by program TRAN1.

Thermal Properties

The temperature calculation subprogram in TRAN1 uses an analytical solution for the flow of heat from a point source moving at a constant velocity across the surface of a body of finite thickness. The solution assumes that the conductivity and volumetric specific heat of the body vary linearly with temperature as follows (Ref. 7):

$$K = K_0\{1+m(T-T_0)\} \quad (1)$$

$$\rho c = \rho c_0\{1+m(T-T_0)\} \quad (2)$$

where

K = conductivity, J/mm°C s;

ρc = volumetric specific heat, J/mm³°C

T = temperature, °C

T_0 = reference temperature, °C

K_0 = conductivity at T_0, J/mm°C s

ρc_0 = volumetric specific heat at T_0, J/mm³°C

m = thermal property gradient, $°C^{-1}$

The following values, taken in conjunction with an assumed arc efficiency of $\eta = 0.55$, were found to give good agreement with previously published data (Ref. 8) on peak temperatures at welds in C-Mn steel specimens: T_0 = 20°C; K_0 = 0.023 J/mm°C s; ρc_0 = 0.004 J/mm³°C; m = 0.0015°C^{-1}.

The reference values of conductivity and volumetric specific heat are typical values for C-Mn steels at ambient temperature. The values of m and η have been selected to give a good fit with measured peak temperature data, and do not necessarily correspond with the actual values of these quantities.

Mechanical Properties

The temperature dependent stress-strain curve of the material in the repair weld was assumed to have the general form shown In Fig. 3. The curve was defined in terms of the five idealized properties σ_0, σ_1, E, E_1, ε_1 shown on fig.1. The model permits each of these properties to be varied with temperature. The nonlinear strain range parameter ε_1 was assumed to have a constant value of 0.005 at all temperatures. The assumed variation with temperature of the remaining parameters is shown in Fig. 4. The room-temperature values of these properties were based on the measured properties of C-Mn weld metal deposited using Tenacito R electrodes. No measurements of the elevated temperature mechanical properties were available, so their assumed variation with temperature was based on that observed in carbon and C-Mn base metals (Ref. 8).

The assumed variation with temperature of the coefficient of thermal expansion is shown in Fig. 5. Two different sets of values were investigated. The "standard" values (solid line) were representative of typical values for carbon-manganese steel (Ref. 8), with a drop in the

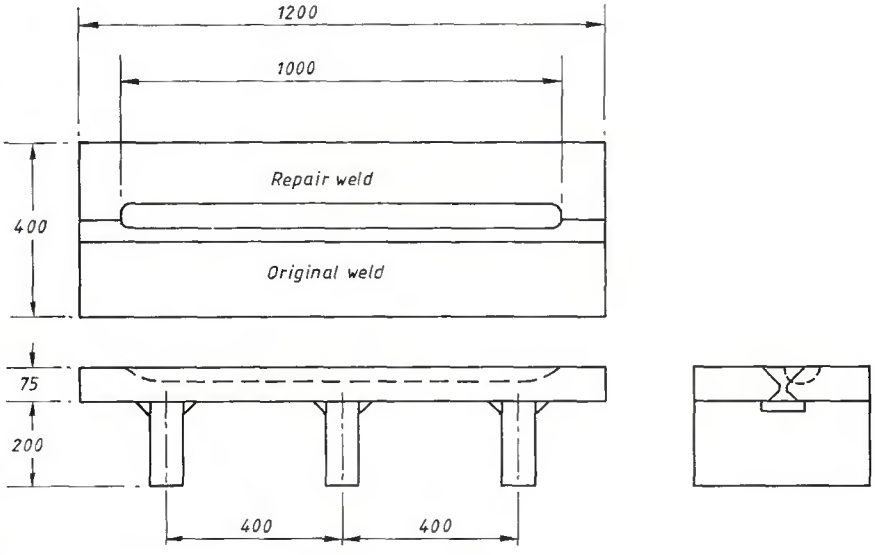

Fig. 1 — Panel W20 schematic.

Table 1—Composition of Materials

Material	C	S	P	Si	Mn	Ni	Cr	Mo	Cu	Ti	Al	O	N
Base plate	0.14	0.019	0.007	0.26	0.89	0.02	0.05	< 0.01	<0.03	<0.003	0.023	0.003	0.007
Original weld	0.07	0.006	0.015	0.23	1.41	0.08	0.06	0.01	0.13	0.006	0.018	0.034	0.012
Repair weld	0.08	0.008	0.010	0.43	1.56	0.02	0.02	0.005	0.02	0.007	<0.003	0.034	0.008

Table 2—Summary of Mechanical Properties

Region	Number of Specimens	0.2% Proof Strength, N/mm^2	Tensile Strength, N/mm^2	% Elongation	% Reduction of Area
Base plate	8	288	433	31	66
Original weld	6	371	494	23	71
Repair weld	6	517	599	19	65

Table 3—Summary of Welding Conditions

Original Weld		Repair Weld	
Type of weld	Double V	Process	SMA
Included angle, side 1, deg	60 (2/3)	Preheat, °C	150
Included angle, side 2, deg	90 (1/3)	Interpass, °C	150
Root opening, mm	0–2	First layer, electrode diameter mm	3.2
Root face, mm	0–2	First layer, current, A	120
Preheat, °C	125	First layer, voltage, V	21–23
Interpass, °C	75–150	First layer, arc energy, kj/mm	0.5–0.8
Restraint	Strongbacks	First layer, number of runs	21
Fill passes, current, A	700	Subsequent runs, electrode diameter mm	4.0
Fill passes, voltage, V	32+	Subsequent runs, current, A	160
Fill passes, travel speed, mm/min	380	Subsequent runs, voltage, V	22–24
Fill passes, arc energy kJ/mm	3.4	Subsequent runs, arc energy kJ/mm	1.2–1.6
Heat treatment, hours at temp/°C	6/600	Subsequent runs, number of runs	63

Fig. 2 — Cross-section of repair weld and original weld in Panel W20.

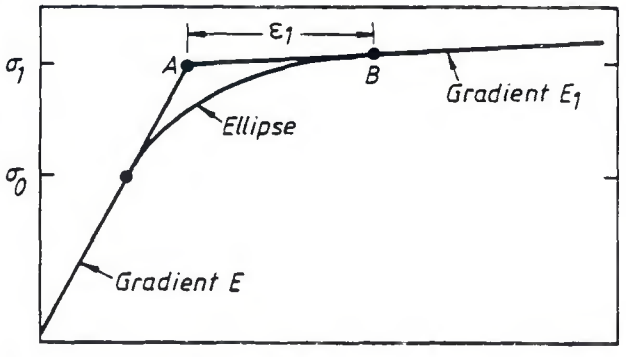

Fig. 3 — Generalized linear-elliptic-linear stress-strain curve.

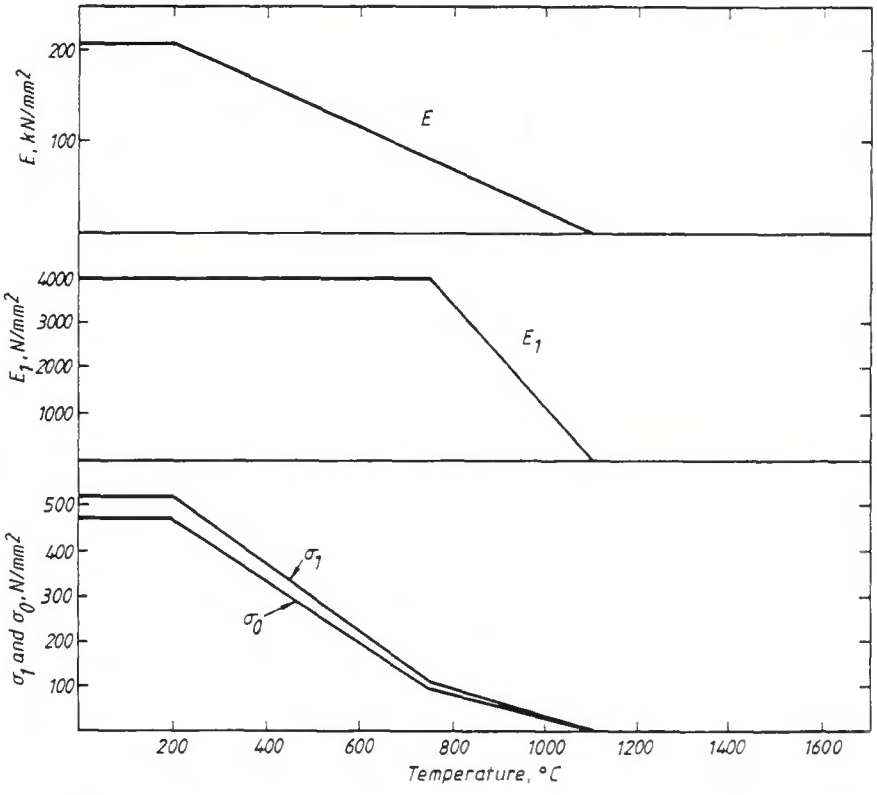

Fig. 4 — Variation of idealized material properties with temperature.

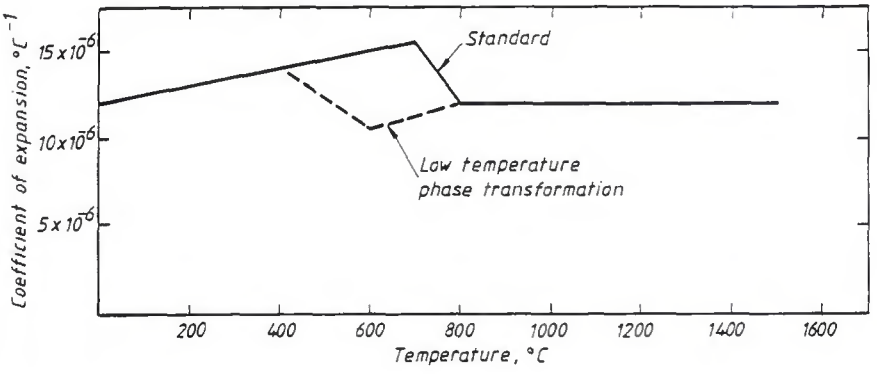

Fig. 5 — Variation of coefficient of expansion with temperature.

coefficient of expansion in the temperature range 700° to 800°C (1292° to 1472°F) caused by a phase change in that range. The "standard" values were used for all the parametric computations presented in this report. The alternative values were used in one trial run to demonstrate the possible effects of a low-temperature phase change in the weld metal in the temperature range 400° to 600°C (752° to 1112°F).

Welding Conditions

The assumed welding conditions for the first and subsequent layers of weld passes were equal to the average values recorded for the weld repair in Panel W20, as listed in Table 3. The program can model the stress and strain changes during each pass of the welding procedure. In practice, it is found that only the first pass in each layer produces significant changes in the stress distribution. Hence, considerable time savings were achieved by only modeling the thermal and stress cycles during one pass of each layer.

Joint Geometry

The typical weld cross-section shown in Fig. 6A was modeled by the simplified element layout shown in Fig. 6B. Joint Element 1 represented the temper bead layer. Elements 2 to 9 represented layers of fill passes. Element 10 represented the first layer of weld passes. Note that the model is essentially one-dimensional and cannot represent the effect of "buttering" the sides of the cavity with low heat input passes. Elements 11 to 16 represented the base metal underneath the repair. At the start of the computer run, only Elements 10 to 16 were assumed to be present. Subsequent elements were added at the start of successive weld layers as appropriate. The effect of removing Element 1, the temper bead layer, after completion of welding, was also included in the model. The depth from the repaired face to the bottom of the fusion zone of the repair weld was 28 mm (1.1 in.).

Structural Restraint

The structural restraint due to the strongbacks in Panel W20 was defined in the model by the following relationships:

$$\sigma_m = \rho\delta + \phi\theta t \quad (3)$$

$$\sigma_b = \tau\delta + \psi\theta t \quad (4)$$

where

σ_m = net membrane stress at section AA (see Figs. 6 and 7), N/mm²

σ_b = net bending stress at section AA, N/mm²

δ = transverse shrinkage at mid-depth, mm

θ = angular distortion, radians

ρ = membrane restraint coefficient, N/mm³

ψ = bending restraint coefficient, N/mm³

ϕ = membrane/rotation restraint coefficient, N/mm³

τ = bending/shrinkage restraint coefficient, N/mm³

t = plate thickness, mm

Satoh and Matsui (Ref. 9) have suggested a system of notation for restraint at welded joints. The terms ρ and ψ above correspond to the parameters I^rF and II^rM, respectively, in Satoh and Matsui's terminology. The cross terms ϕ and τ have been introduced in the present project to allow for the interactive membrane/bending effects that occur when the restraint is applied by strongbacks to one face of the welded specimen.

The values of all four restraint coefficients were determined using a

finite element model of the weld panel cross-section — Fig. 7. As the model was two-dimensional, the effect of the strongbacks was effectively "smeared" along the length of the panel. This simplification was justified by the fact that there did not appear to be any longitudinal variations In the measured transverse residual stresses at the strongback positions in Panel W20 (Ref. 1). Two load cases were run, one with uniform displacement at AA and one with uniform rotation. The values of the restraint coefficients were derived from the computed net forces and moments on AA, and had the following values:

$\rho = 92.5$ N/mm^3

$\phi = -81$ N/mm^3

$\tau = -486$ N/mm^3

$\psi = 669$ N/mm^3

Results and Discussion

The computed through-thickness distribution of transverse residual stresses on the repair weld centerline is plotted in Fig. 8 and compared with distributions measured at two locations in Panel W20 (Ref. 1). It can be seen that the overall shape of the computed distribution agrees well with that of the measured stresses, and that there is also very good agreement on the level of stress in the compressive region and on the depth of the tensile region. On the other hand, the program has overpredicted the tensile stresses, both in the repair weld and at the back of the plate.

The alternative computed distribution assuming a low-temperature phase change was very similar to that computed using "standard" material behavior. There was a slight reduction in the tensile stresses in the weld, probably caused by the reduced thermal strains in the range 400° to 800°C (752° to 1472°F). However, the assumed phase change temperature range was not low enough to reduce the peak stress at the surface significantly below yield. Better agreement with the experimental results in this region could have been obtained either by assuming a lower phase change temperature or by taking a lower value for the stress parameter σ_1, which corresponds approximately to the weld metal yield or proof strength. However, measurements on the repair surface after removal of the temper beads showed that localized peak stresses up to weld metal yield could occur. Hence, for the purposes of providing an upper bound to

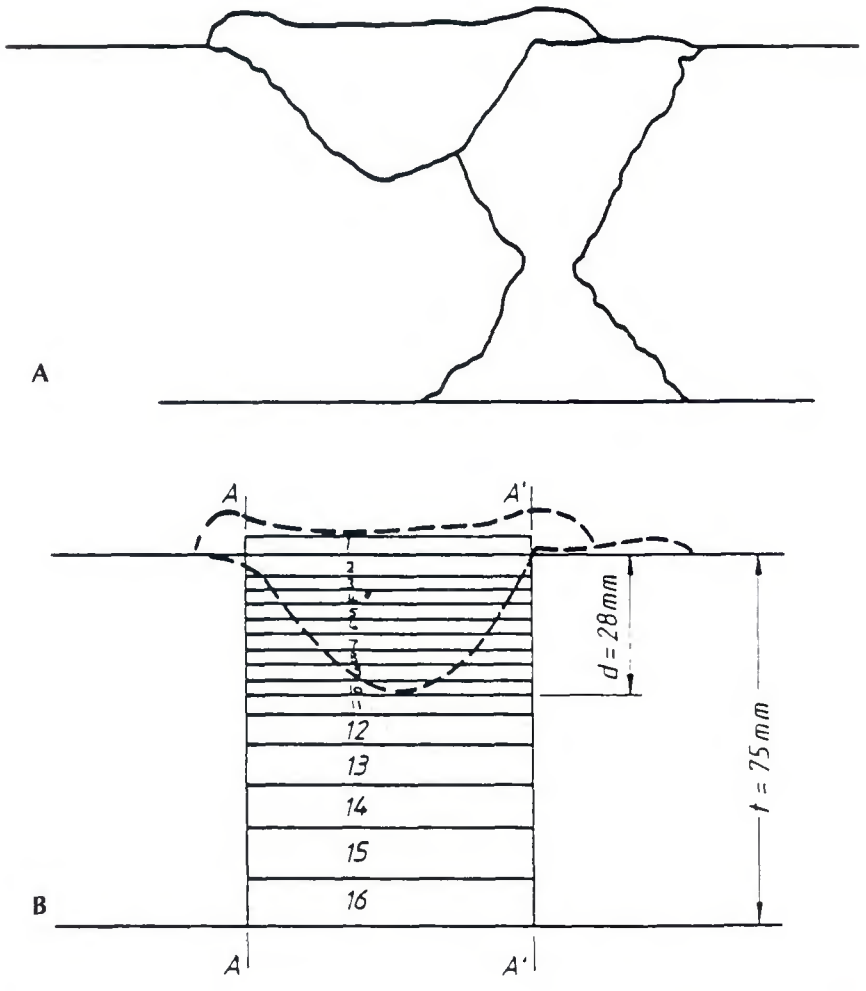

Fig. 6 — A — Profile of original and repair welds in Panel W20; B — representation of repair weld in computer model.

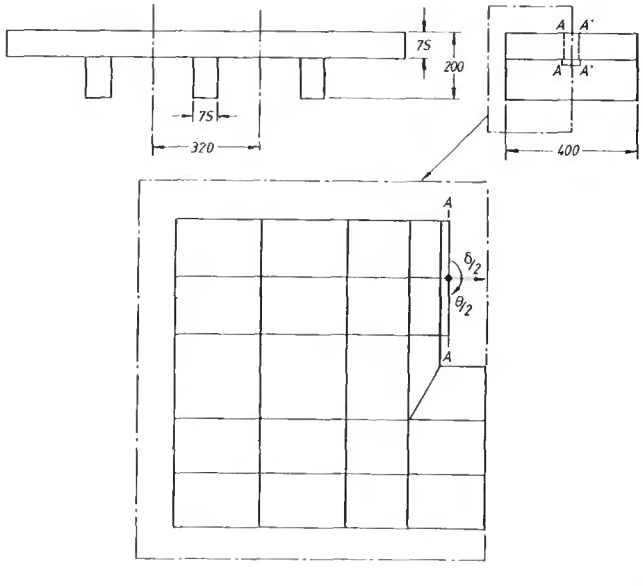

Fig. 7 — Finite element model used to calculate restraint at repair weld in panel with strongbacks.

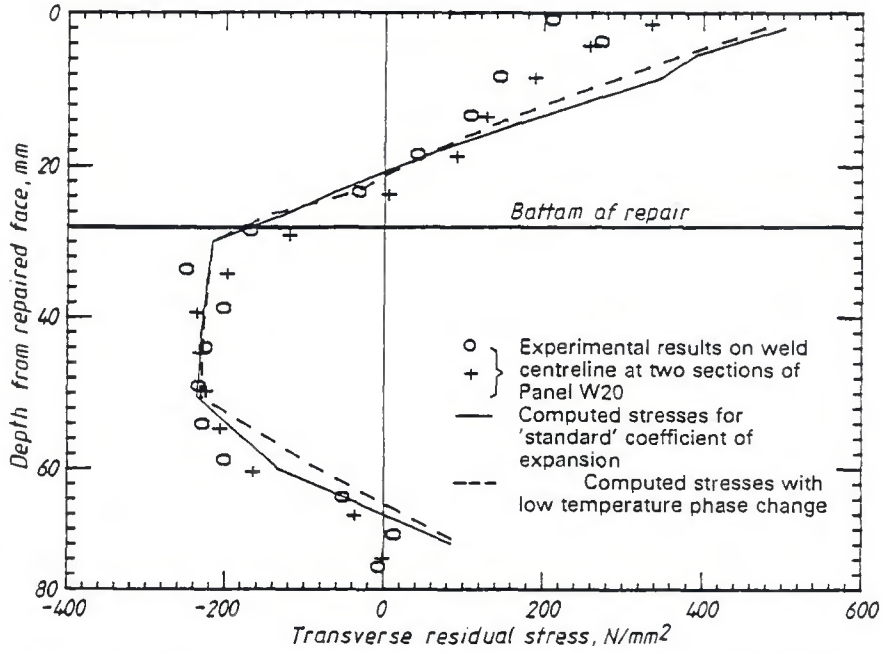

Fig. 8 — Comparison of computed and measured stresses at 28-mm-deep repair weld in 75-mm-thick specimen.

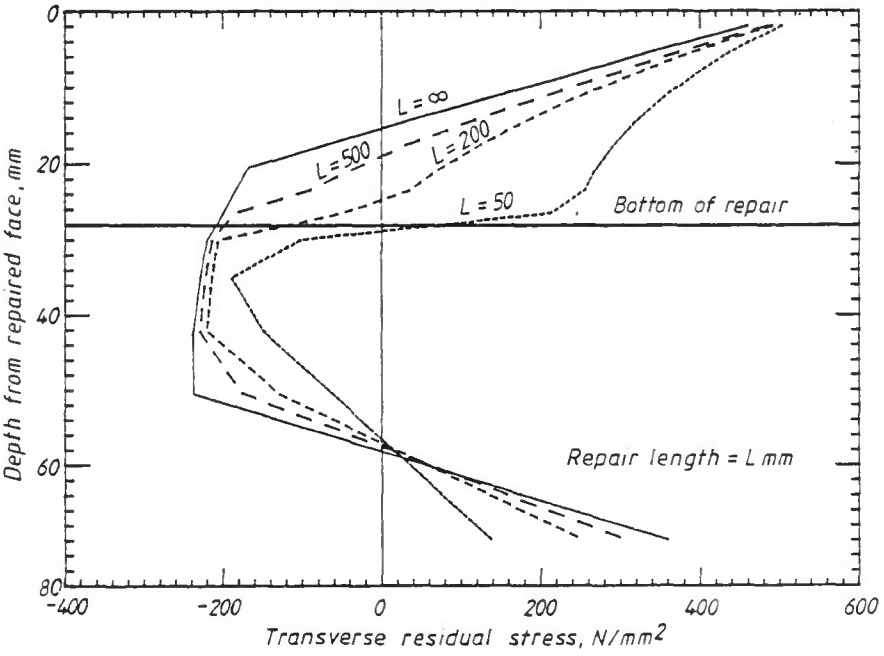

Fig. 9 — Computed residual stresses at midlength of repair on infinite plate (repair depth 28-mm, wall thickness 75 mm).

these localized stresses, it is appropriate to continue to use the weld metal yield strength and the "standard" coefficient of expansion in the computer model.

The low level of measured stresses at the back of the plate may have been caused by stresses remaining in the plate after postweld heat treatment (PWHT) and before repair welding. The stress level in this region is not relevant to the integrity of the repair weld.

Due to the presence of external restraint, the stress distributions shown in Fig. 8 are not balanced across the section thickness. They have the following net reaction components: measured membrane stress –50 N/mm², computed membrane stress –17 N/mm², measured bending stress +184 N/mm², computed bending stress +180 N/mm².

The computed bending stress agreed closely with the measured value, whereas the computed membrane stress was less compressive than the measured value due to the overprediction of tensile stresses in certain regions, as discussed above. It is interesting to note that, despite this discrepancy, both measured and computed values of the membrane stress across the repaired section were compressive. At the time the original measurements were made, it was not apparent to the author how there could be a net compressive force across the weld. The present analysis shows that this was made possible by the fact that the membrane/rotation coefficient ϕ had a negative value. The positive angular distortion at the repair generated a compressive membrane stress that outweighed the tensile membrane stresses due to transverse shrinkage. The prediction of negative membrane stresses by the program is an example of how such models are capable not only of providing quantitative comparisons with experimental results, but also of giving a qualitative insight into previously unexplained phenomena.

Parametric Survey

Introduction

The ability of computer program TRAN1 to model the stress distribution at a 28-mm-deep repair weld in a 75-mm-thick panel restrained by strongbacks was demonstrated in the previous section of this paper. In this section, the use of the program to calculate the residual stress distribution for a range of restraint conditions representative of those that might be found at a repair in a pressure vessel will be described. The program was first used to model the type of restraint present at the center of a repair

of finite length in an infinite flat plate. It was then used to investigate the effects of curvature at a repair in a vessel wall. Finally, it was used to consider the effect of repair depth and wall thickness on the residual stress distribution.

Effect of Repair Length

The restraint at a weld of finite length in an infinite flat plate is a function of the weld length and varies along the length of the weld. The local restraint coefficients at a distance x from the middle of the length of the repair is defined below.

The membrane restraint coefficient $\rho(x)$ is equal to the reciprocal of the transverse shrinkage $\delta(x)$ at x due to uniform unit membrane stress across the weld over its entire length.

The bending restraint coefficient $\psi(x)$ is equal to the reciprocal of the product of the plate thickness t and the angular distortion $\theta(x)$ at x due to uniform unit bending stress across the weld over its entire length.

Hence:

$$\rho(x) = \mathrm{I'FB} = \frac{\sigma_m}{\delta(x)} \quad (5a)$$

$$\psi(x) = \mathrm{II'MB} = \frac{\sigma_b}{t\theta(x)} \quad (5b)$$

$$\tau(x) = 0 \quad (5c)$$

$$\phi(x) = 0 \quad (5d)$$

The r terms are the equivalent parameters in the restraint terminology suggested in (Ref. 9). It should be noted that for the purposes of the above definitions the repaired structure is considered to be divided into two parts: the repair region, including the underlying base metal and original weld metal; and the surrounding structure. The restraint coefficients describe the elastic behavior of the surrounding structure, and they are independent of the depth of the repair weld. In the case of a repair in a flat plate, the membrane stresses in the surrounding structure due to the in-plane displacements at the edge of the repaired region are analogous with those in a through-cracked panel due to displacements of the crack face. The membrane restraint coefficient at a repair weld can be evaluated using existing solutions for the displacement at the crack face due to uniform crack face pressure. These displacements can in turn be shown, using the principle of superposition, to

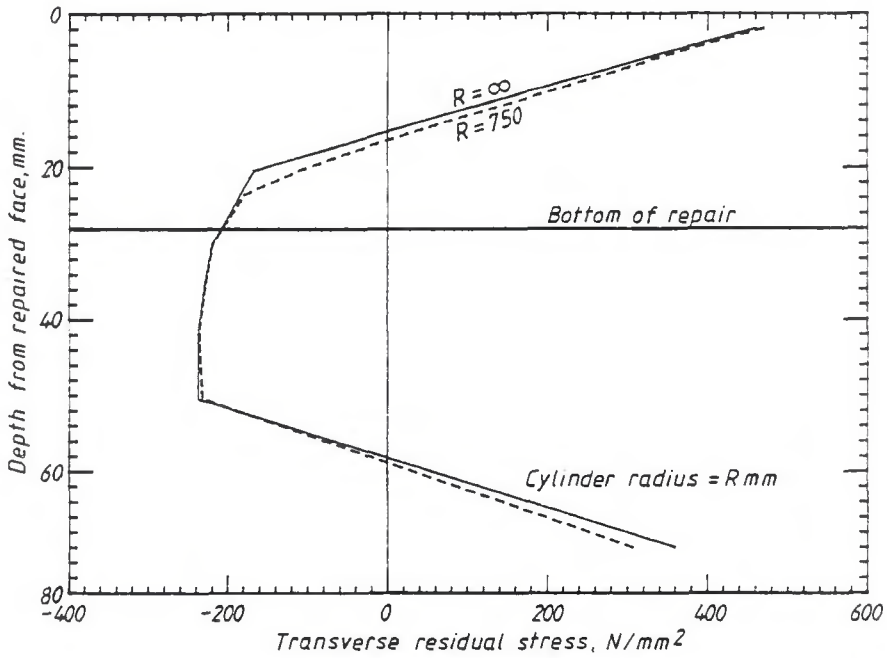

Fig. 10 — Computed residual stresses at full length axial repair in cylinder (repair depth 28 mm, wall thickness 75 mm).

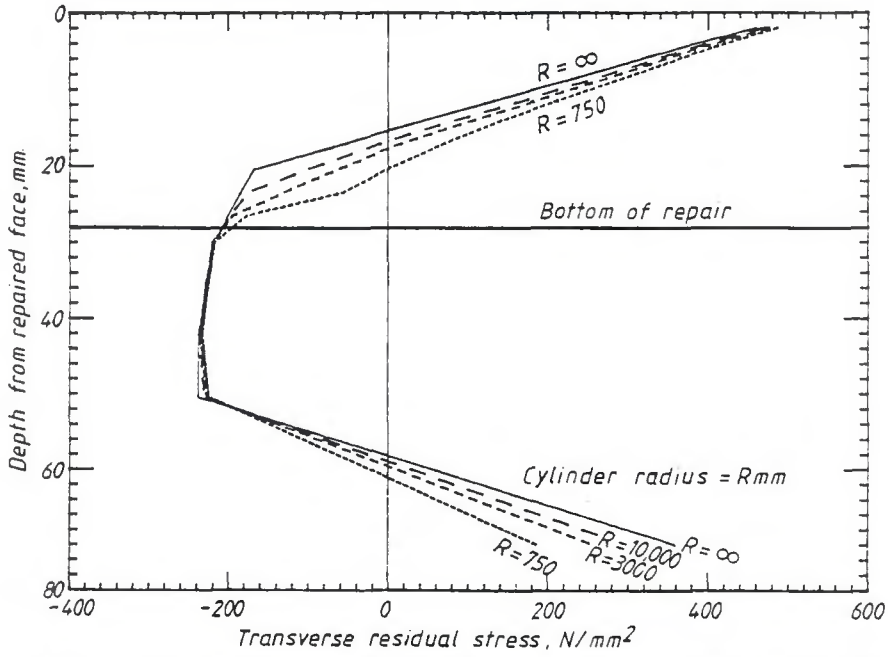

Fig. 11 — Computed residual stresses at full circumferential repair in cylinder (repair depth 28 mm, wall thickness 75 mm).

be equal to those caused by an externally applied uniform membrane stress equal to the crack face pressure. The crack face displacement at a through-thickness crack in an infinite plate under uniform membrane stress is given by Westergaard (Ref. 10):

$$\delta(x) = \frac{4\sigma_m\sqrt{c^2 - x^2}}{E'} \qquad (6)$$

where E′ is E under plane stress conditions, c is the crack or repair half length, and x is the distance along the crack from its center.

Hence, by combining (5a) and (6),

$$\rho(x) = \frac{E}{4\sqrt{c^2 - x^2}} \qquad (7)$$

There does not appear to be a readily available solution for the local bending restraint. However, for certain simple loading conditions, it can be shown that the bending restraint coefficient is equal to half the membrane restraint coefficient. These conditions include the restraints at a ring weld in a flat plate, and at a full width weld in a plate whose edges parallel with the weld are fully restrained and whose edges perpendicular to the weld are restrained against movement perpendicular to the weld. The general solutions for membrane and bending stresses in flat plates are closely analogous. It is here assumed that the bending restraint is in general equal to half the membrane restraint, provided that the membrane and bending boundary conditions are equivalent. This would be the case in an infinite flat plate. Hence:

$$\psi(x) = \frac{E}{8\sqrt{c^2 - x^2}} \qquad (8)$$

At the middle of a repair weld, x = 0, and;

$$\rho(0) = 2\psi(0) = \frac{E}{4c} = \frac{E}{2L} \qquad (9)$$

Program TRAN1 has been used to calculate stress distributions at the middle of repair welds of various lengths between 50 mm and infinity. The weld depth, plate thickness, welding procedure and repair weld metal properties were identical to those previously used for the validation exercises, as previously described. The computed residual stresses for repairs in infinite flat plates are plotted In Fig. 9. It can be seen that the distributions all have a tension-compression-tension pattern, with stresses tending to the repair weld metal yield strength, 520 N/mm² (75.4 ksi), at the repaired surface, and then falling off with depth from the surface. The stress gradient decreases and the depth of tensile zone increases as the repair length decreases.

Effect of Vessel Radius and Repair Orientation

The effect of vessel radius on the restraint, and hence on the residual stress distribution at a repair weld in a cylindrical vessel, has been investigated for three repair configurations: 1) full length axial repair, 2) full circumferential repair, and 3) part-circumferential repair; length L = 200 mm (7.9 in.).

The formulas used to evaluate the restraint coefficients for each configuration are summarized in Table 4. The formulas for the restraint coefficients at a full length axial repair were obtained using simple bending theory, assuming that radial/axial planes remained planes. Although all four restraint coefficients are nonzero, only ψ is significant for thin-walled cylinders. For full circumferential repairs, only ψ is nonzero. Its value was determined on the basis of elastic thin cylinder theory (Ref. 11), and is valid for R ≥ 10t. The restraint at the midpoint of a part-circumferential flaw was obtained by simply adding together the formulas for a short defect in a flat plate and for a full circumferential defect in a cylinder. The combined formulas tend to the appropriate values for the limiting cases as R or L tend to infinity, but may overestimate the total restraint present when the two components are of comparable magnitude.

Program TRAN1 was used to calculate the residual stress distributions for the standard 28-mm-deep repair in 75-mm wall thickness vessels of radii between 750 mm (29.5 in.) and infinity. The computed stress distributions for full length axial repairs are shown in Fig. 10. The restraint at this type of repair is low, and hence the residual stresses are similar to those in an unrestrained weld, and are insensitive to vessel radius. The restraint is higher at a full circumferential repair, due to the inherent bending stiffness of the cylinder in the axial direction, and the depth of the tensile zone increases as the cylinder radius decreases — Fig. 11. At a short part-circumferential repair (Fig. 12), the restraint due to weld length is more significant than that due to the bending stiffness of the cylinder, and there is a deep tensile zone regardless of the vessel radius.

The depth of tensile zone for the three types of repair are plotted on Fig. 13 as a function of vessel radius. The figure shows that, even for the worst possible case of a short part-circumferential repair in a cylinder with a small radius, the tensile zone was always computed to be less deep than the repair weld, for a 28-mm-deep repair in 75-mm wall thickness. Figures 10 to 12 show that, for all cases considered, the transverse stresses varied approximately linearly with depth from the repair weld metal yield stress at the surface to the point (within the depth of the repair) where they fall to zero.

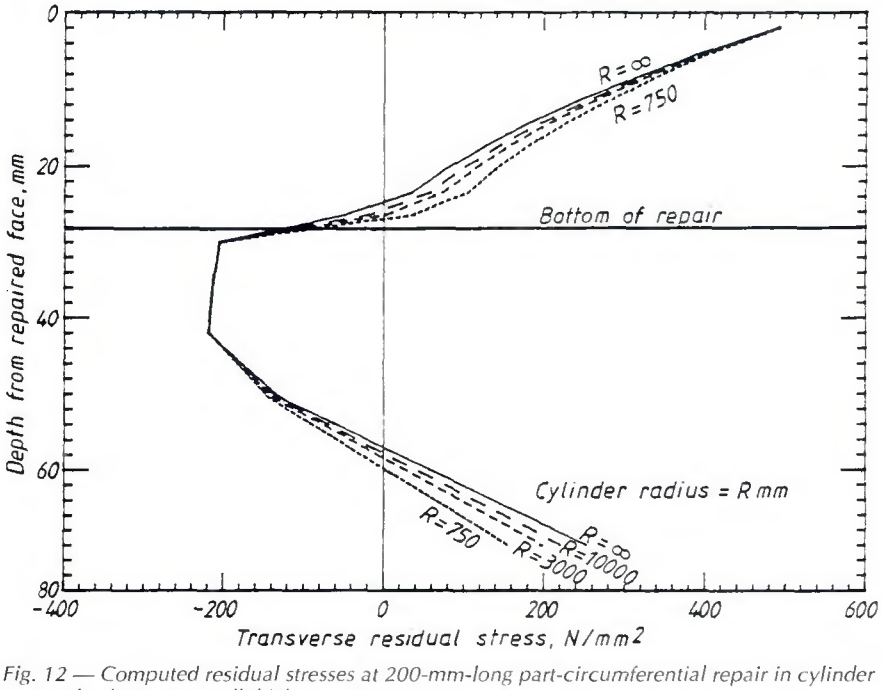

Fig. 12 — Computed residual stresses at 200-mm-long part-circumferential repair in cylinder (repair depth 28 mm, wall thickness 75 mm).

Table 4—Formulaes Used to Calculate Restraint Coefficients

Coefficient	Midpoint of Repair in Flat Plate	Full Length Axial Repair in Cylinder	Full Circumferential Repair in Cylinder	Midpoint of Part Circumferential Repair in Cylinder
In-plane, ρ	$\frac{E}{2L}$	$\frac{Et^2}{12\pi R^3(1-\nu^2)}$	0	$\frac{E}{2L}$
Out-of-plane, ψ	$\frac{E}{4L}$	$\frac{3E}{4\pi R(1-\nu^2)}$	$\frac{E[3(1-\nu^2)]^{1/4}}{4(1-\nu^2)(Rt)^{1/2}}$	$\frac{E}{4L}+\frac{E[3(1-\nu^2)]^{1/4}}{4(1-\nu^2)(Rt)^{1/2}}$
Membrane rotation, ϕ	0	$\frac{-Et}{12\pi R^2(1-\nu^2)}$	0	0
Bending shrinkage, τ	0	$\frac{-Et}{2\pi R^2(1-\nu^2)}$	0	0

Effect of Wall Thickness

Computer program TRAN1 has been used to calculate the transverse residual stresses for 28-mm-deep repair welds with wall thicknesses of 28, 50, 75, 150 and 300 mm (1.1, 2, 3, 6 and 11.8 in.). A repair configuration was selected that gave the highest practical level of restraint, namely, a 200-mm-long part-circumferential repair in a cylindrical vessel of radius equal to ten times the wall thickness. All welding conditions and material properties were as used for the validation run described previously.

The computed stress distributions for the five wall thicknesses investigated are shown in Fig.14. For all thicknesses, except 28 mm, the distributions showed the usual overall pattern of tensile stresses in the repair, with compressive stresses at mid-depth and tension at the back face. In the medium thickness plates (50 and 75 mm), the stresses decreased approximately linearly from the repair weld metal yield strength at the repaired surface to zero close to the bottom of the repair. The stresses were more tensile in the very thick plates (150 and 300 mm), decreasing gradually with distance from the surface and then dropping rapidly at the bottom of the repair.

The computed stresses for the 28-mm-thick cylinder illustrate the type of distribution to be expected at a full depth repair under high restraint. The tensile zones at the back and front surface of the plate interacted, such that there was no compressive zone at mid-depth, even though the stresses fell more rapidly near the front surface than was the case in thicker material.

The results in Fig. 14 represent the stresses associated with the highest practical level of restraint at repair welds. The computations for thicknesses of 28, 75 and 300 mm were repeated for full length axial repairs in large radius cylinders, which may be regarded as giving the lowest practical level of restraint. The radius was set at 40 times the wall thickness. The computed distributions are shown on Fig. 15. The distribution for the 300-mm-thick case was virtually identical to that for the highly restrained case. This occurred because the internal restraint due to the massive thickness of the material under the weld was so large that external structural restraint was irrelevant. The stress distribution in the 75-mm-thick cylinder under low restraint was typical of those shown in Fig.10 and discussed previously. In the 28-mm-thick cylinder, there was no material under the weld and the stress distribution was sensitive to external restraint. The full length, full depth repair was effectively a single-sided groove weld, and the computed distribution was typical of those found in lightly restrained groove welds. There was a tensile peak at the repaired surface, balanced by compressive stresses at mid-depth and another tensile peak at the back face.

Effect of Repair Depth

The program was used to compute the transverse residual stresses for repairs 10, 28 and 46 mm (0.4, 1.1 and 1.8 in.) deep in 75-mm-thick material. As in the previous section, the analysis was applied to the highly restrained case of a short, part-circumferential repair in a vessel of radius equal to ten times the

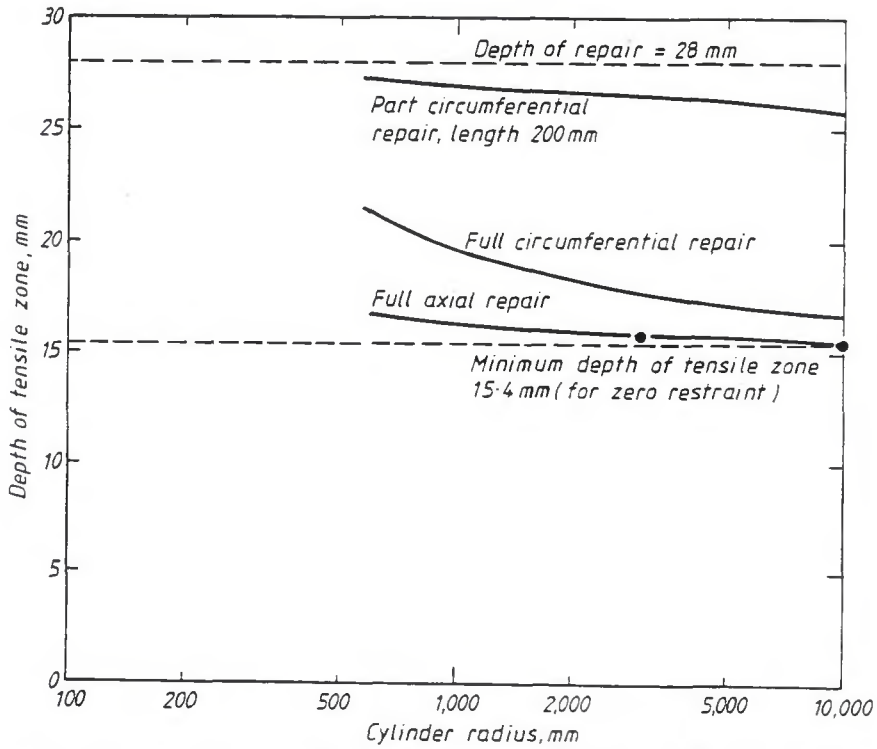

Fig. 13 — Variation of computed depth of tensile zone with cylinder radius for 28-mm-deep repair in 75-mm wall thickness.

wall thickness, 75 mm. The repair lengths were assumed to be 70, 200 and 300 mm (2.8, 7.9 and 11.8 in.), giving in each case an aspect ratio of about 7:1. The repair widths were also scaled in proportion with the depths, giving a width-to-depth ratio of approximately 2:1 in each case. The welding procedures were based on those used previously, with three layers of weld passes plus the temper bead layer in the 10-mm-deep repair, and fifteen layers plus the temper bead layer in the 46-mm-deep repair.

The computed stress distributions are shown in Fig. 16. It can be seen that the depth of the tensile zone increased as the depth of repair increased, though not necessarily proportionately. The stresses in the 10-mm-deep repair were at tensile yield strength of the repair weld metal at the surface, and decreased slowly with the depth to about 360 N/mm^2 (52.2 ksi) at the bottom of the repair, falling to zero 3 mm (0.12 in.) below the repair. The stresses in the 46-mm-deep repair were below yield at the surface at about 370 N/mm^2 (53.6 ksi). It is not known why this occurred, but it may have been associated with the particular repair depth to plate thickness ratio for this case. The stresses decreased slowly with depth, and retained a significant tensile value (over 100 N/mm^2 – 14.5 ksi) to within 4 mm (0.16 in.) of the bottom of the repair.

Discussion

The computed stress distributions described previously indicated that the transverse residual stresses at a 28-mm-deep repair in 75-mm-thick material decreased approximately linearly with depth from the repaired surface, and always fell to zero within the depth of the repair, regardless of the level of restraint at the joint. Unfortunately, the results from subsequent sections suggested that this conclusion could not be generalized to include other depth-to-thickness combinations. For repair welds with depths less than 30% or more than 50% of the plate thickness, in most cases the stresses did not decrease linearly within the depth of the repair, and retained a significant tensile value near to the bottom of the repair.

The results suggested that the occurrence of stress distributions which varied approximately linearly within the repair depth is limited to a small range of repair depth-to-thickness ratios, possibly $0.3 < d/t < 0.5$. The generation of guidelines for stress distributions at repair welds outside this range would require additional investigation using the computer model, supported by some additional experimental studies of relevant repair geometries.

It is possible that some of the predictions of the computer model are pessimistic and that future measurements will show that the transverse stresses are less tensile than the computed results. A number of conservatisms have been built into the model itself and into the assumed values of the material properties and restraint coefficients. Rigid boundaries were assumed to exist at the edges of the repair weld (Fig. 6B), which tended to inhibit the redistribution of stresses in the section, and hence, effectively increased the restraint. The transverse residual stresses were allowed to have a maximum value equal to the weld metal yield strength, even though it was known from previous results (Ref. 1) that yield magnitude stresses only occur in practice at very localized positions, and cannot exist as a bulk value over a significant depth, due to yielding of the adjacent base metal. The calculated restraint coefficients at part-circumferential repair welds may also have been conservative.

Despite these conservatisms, and the lack of direct experimental evidence to validate the prediction for very shallow or very deep repairs, the present results are supported by experimental measurements in analogous welding configurations. The deposition of a thin layer of

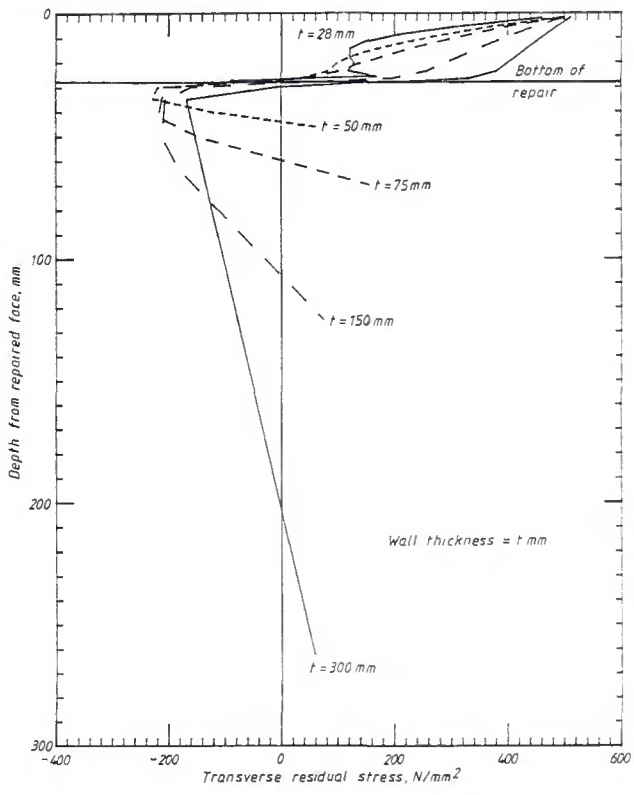

Fig. 14 — Variation of residual stress distribution with wall thickness at 28 mm.

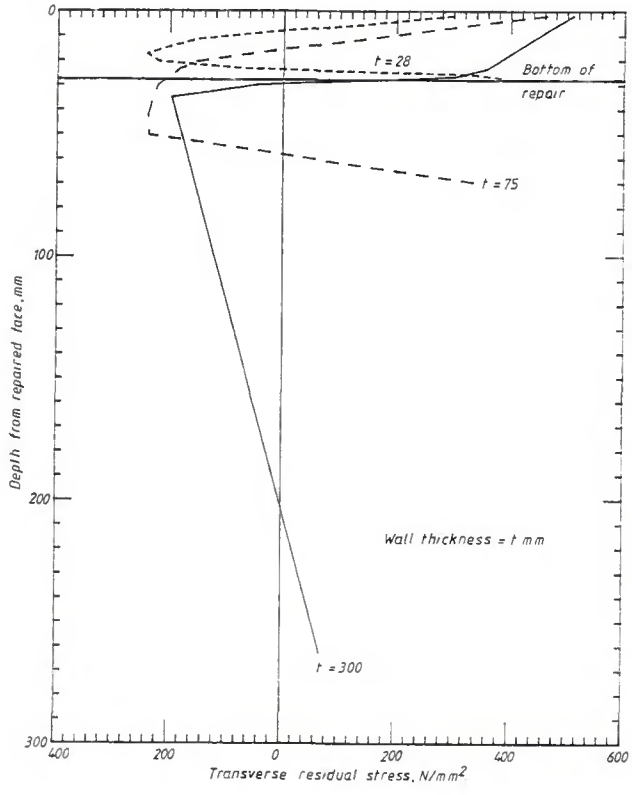

Fig. 15 — Variation of residual stress distribution with wall thickness at 28-mm-deep repair with low restraint.

cladding on thick pressure vessels has similarities with the case of a large, shallow repair in a thick base material. Measurements of residual stresses, (Refs. 12, 13) in clad specimens have shown that the residual stresses were tensile throughout the depth of the weld metal and for some depth in the underlying base metal. This supports the prediction that tensile transverse stress could exist below a shallow repair weld in a thick base metal — Figs. 14–16.

Masubuchi (Ref. 14) presented measurements of transverse residual stresses, averaged through the thickness, at short full-depth repair welds in flat plate specimens which he referred to as "slit-type" specimens. The residual membrane stress across a 200-mm-long slit weld at the center of its length was 200 N/mm² (29 ksi), which compares closely with the calculated mean membrane stress for the 200-mm-long full depth repair weld in 28-mm-thick material shown in Fig. 14, which was 194 N/mm² (28.1 ksi). These observations from analogous welding configurations give increased confidence in the reliability of residual stress distributions computed by TRAN1 for repair configurations for which no direct experimental validation is available.

Goldak (Ref. 15) has published a review of modeling of thermal stresses and distortion in welds. The computer model described in the present paper is much simpler than that adopted by most other workers. The potential disadvantage of using a simple model is that there is a greater potential for errors associated with the simplifying assumptions. Experiments must be used to demonstrate the applicability of the model for each new class of weldments under investigation. The advantage of using a simple model is that it requires much less computing resources, allowing an extensive parametric survey to be conducted. This type of survey increases understanding of the relationship between residual stresses, welding conditions and structural geometry. In the present case, the model (without any recalibration or "tweaking") has given good agreement with a measured distribution, has produced results which are compatible with published observations in related repair configurations, and has provided a qualitative explanation of a previously unexpected and unexplained phenomenon, the occurrence of a compressive membrane residual stress in a repair weldment.

In this investigation, TRAN1 has not been used to investigate the effect of material properties on residual stresses at repair welds because it was believed that there was insufficient data on elevated temperature properties to justify such a study. Additionally, the program does not model the yield of base metal adjacent to the repair zone, which may influence the final stress state. As previously discussed, the use of repair weld metal mechanical properties in the model gives rise to peak surface stresses of weld metal yield magnitude, which corresponded with previous experimental observations (Ref. 1). The investigation was based on the mechanical properties of carbon-manganese weld metal. It is anticipated that similar analyses based on the properties of other metals would also produce peak stresses equal in magnitude to their respective yield strengths.

One observation from the present investigation that is not apparent from the stress plots is that, before removal of the temper beads, the residual stresses were at repair weld metal yield magnitude at the surface of the temper bead, and decreased with depth to a lower value at plate surface level. However, when the temper beads were removed, the residual stresses were redistributed such that the stresses at the new surface were raised to yield level.

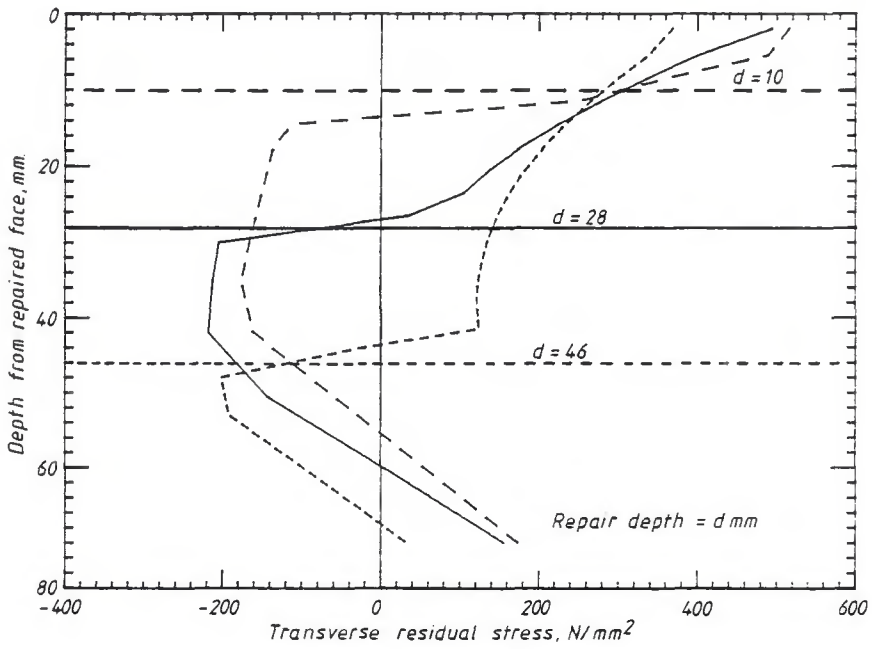

Fig. 16 — Variation of residual stress distribution with repair depth in 75-mm wall thickness with high restraint.

Conclusions

Computer program TRAN1 has been used to investigate the effect of structural restraint, repair depth and plate thickness on transverse residual stresses at repair welds. The program was found to give good agreement with experimental results for a 28-mm-deep repair weld in a 75-mm-thick aluminum treated carbon-manganese test panel, and also accounted for the experimental observation that the net membrane stresses in the panel at the repair were compressive.

Computed stress distributions for a particular repair procedure in a range of structural configurations, including repairs of different lengths in flat plates, and full length axial, full circumferential and part-circumferential repairs in cylinders, showed that the transverse residual stresses decreased approximately linearly from yield value at the repaired surface to zero at some point within the depth of the repair.

Analysis of repairs of different depths indicated that the above description of the stress field was only applicable for repairs whose depth was between about 30% and 50% of the wall thickness. At shallower repairs, the computed transverse stresses had a significant tensile value at the bottom of the repair, due to the high inherent restraint of the underlying material. At deeper repairs, there were increased tensile stresses at the bottom of the repair due to the influence of the secondary tensile peak stress at the back surface.

Acknowledgments

The author is grateful to B. A. Martin, D. Jarvis and N. Cann, who carried out the residual stress measurement on the repair welded panels, and for the advice and cooperation of other members of the project team, in particular N. Bailey, H. G. Pisarski and. R. L. Jones.

This work was funded jointly by research members of The Welding Institute, the Minerals and Metals Division of the U.K. Department of Trade and In-

dustry, and members of the 5532 Sponsor Group.

References

1. Leggatt, R. H. 1986. Residual stress measurements at repair welds in pressure vessel steels in the as-welded condition. Welding Institute Research Report 315/1986.

2. Leggatt, R. H. 1987. Residual stresses and distortion in multipass butt welded joints in Type 316 stainless steel. Residual Stresses in Science and Technology. Proceedings, International Conference on Residual Stresses, Garmisch-Partenkirchen, Germany, 15-17 October 1986. Eds E. Macherauch and V. Hauk, Publ. D-6370 Oberursel 1, Germany, Deutsche Gesselschaft für Metallkunde.

3. Alberry, P. J., Myera, J., and Chew, B. An improved welding technique for HAZ refinement. *Welding and Metal Fabrication*, 45 (9):549, 551, 553.

4. Alberry, P. J., Rowley, T., and Yapp, D. 1978. Control of MMA weld quality by deposition sequence. Paper 18, 4th Intl. TWI Conf.: Advances in welding processes, pp. 105–116.

5. Alberry, P. J., and Jones, W. K. C. 1977. Diagram for the prediction of weld HAZ. Metals Tech 4 (7):360–364.

6. Rosenthal, D., and Norton, J. D. 1945. A method of measuring triaxial residual stresses in plates. *Welding Journal* 24 (5):295-s to 307-s.

7. Grosh, R. T., Trabant, E. A., and Hawkins, G. A. 1955. Temperature distributions in solids of variable thermal properties heated by moving heat sources. Q. Appl. Maths 13(2).

8. Leggatt, R. H. 1980. Distortion in welded steel plates. Ph.D. thesis, Cambridge University.

9. Satoh, K., and Matsui, S. 1978. Notation system of joint restraint severity. IIW Doc. X-910-78.

10. Westergaard, H. M. 1939. Bearing pressures and cracks. *J. Appl. Mech* 60 (9):A49.

11. Timoshenko, S., and Woinowski-Krieger, S. 1959. *Theory of Plates and Shells*. McGraw Hill.

12. Schimmoeler, H. A., and Ruge, J. L. 1977. Estimation of residual stresses in reactor pressure vessel steel specimens clad by stainless steel strip electrodes. Residual Stresses in Welded Construction and their Effects, Proc. Intl. Conf. The Welding Institute.

13. Vinckier, A. G., and Pense, A. W. 1974. A review of underclad cracking in pressure vessel components. WRC Bulletin 197.

14. Masubuchi, K. 1980. *Analysis of Welded Structures*. Pergamon Press.

15. Goldak, J. 1989. Modeling thermal stresses and distortions in welds. Proc. 2nd Int. Conf. on Trends in Welding Research, Gatlinburg, Tenn., pp. 71–82.